H-Ar potential from high-resolution differential cross-section measurements at thermal energy*

D. Bassi,† M. G. Dondi, F. Tommasini, F. Torello, and U. Valbusa
Istituto di Scienze Fisiche dell'Università, Genova, Italy
(Received 8 April 1975)

We report high-resolution differential cross-section measurements for the systems H-Ar and D-Ar at a relative energy of 67 meV. The primary beam is velocity selected (FWHM 10%) and the secondary beam is produced by a low-temperature source. The experimental resolution allows us to resolve the "fast-oscillation" structure of the cross section. Our experimental results are compared with the effective cross sections obtained from potentials recently proposed for these systems. The present data cannot accommodate the potential forms deduced from two separate measurements of the energy dependence of the total cross section, but are not in disagreement with the recent theoretical results of Wagner, Das, and Wahl. The sensitivity of the measured properties to the attractive and to the weakly repulsive parts of the potential is discussed, and we show that a compensation effect between the two does not allow a unique determination of the potential.

I. INTRODUCTION

The low-energy repulsive interaction and the Van der Waals minimum have been recently predicted by *a priori* calculations for the simplest atom-atom closed-shell He_2 system[1] and for the open-shell H-He,[2] H-Ne,[3] and H-Ar[4] systems. A common feature of these interactions is a well of small depth which contains zero or one bound state. H-He and He-He have an extremely shallow well ($\epsilon \lesssim 1$ meV) while systems like H with heavier rare gases have considerably deeper wells ($\epsilon \sim 5$ meV).

The information on these interactions, derived from experimental data, can provide a useful test of quantum chemical theories. Molecular-beam scattering experiments are regarded as the most direct method for investigating the interaction of systems which do not form a stable compound.[5]

The best-known system is He_2, essentially because scattering, equilibrium, and transport data over an extended energy range have been reported in the literature.[6] The low-energy repulsive part up to 0.14 eV, as determined by inversion of high-resolution total-cross-section measurements,[7] is in good agreement with theoretical calculations[1] and with the potential derived from differential-cross-section experiments.[8] At energies smaller than the well depth the relative differential cross sections are almost isotropic and are therefore almost insensitive to the potential, while the total cross section shows an atomic Ramsauer-Townsend minimum. Experimental evidence for this effect and a preliminary analysis were recently published,[9] but a unique determination of the attractive potential seems impossible for "extreme" quantum systems.[10]

Experimental data for H–rare-gas systems are quite limited. The total cross sections are the main source of information. The repulsion at small internuclear distance was derived from high-energy data.[11,12] Some indication of the strength parameter of the potential ϵr_m (r_m is the equilibrium separation distance) is given by the pioneering experiment of Fluendy *et al.*[13] More recent scattering experiments at thermal energies[14,15] were analyzed with two or three parameter potentials. Because of the lack of structure of these measurements, the analysis is greatly affected by the error in the determination of the absolute cross section. More information can be derived from high-resolution total-cross-section experiments at lower energies where the quantum system H-He undergoes a Ramsauer-Townsend effect[16] and the more classical H–heavier-rare-gas systems show orbiting[17] and possibly glory structure, or from high-resolution differential-cross-section experiments at thermal energies.

Until now high-resolution differential measurements were not performed because of experimental problems in the production, velocity selection, and detection of atomic hydrogen beams. We have recently developed experimental techniques which allow us to resolve clearly the predicted fast quantum oscillations of the differential cross section.[18] Preliminary results for H-H_2 and D-H_2 were previously reported.[19] In this paper we present some data for the systems H-Ar and D-Ar. Our experimental results are compared with the effective cross sections obtained from potentials recently proposed for these systems. A new potential is suggested.

II. EXPERIMENTAL SETUP

A schematic diagram of the apparatus is shown in Fig. 1. An atomic beam of hydrogen or deu-

terium is produced by the rf source S (diameter 0.4 mm, pressure 0.5 torr, measured degree of dissociation better than 90%). The atomic beam, chopped (30 Hz) and velocity selected by a magnetic lens system ML, crosses at right angles the secondary beam produced by a multichannel effusive source A at a temperature of about 100 °K. The dimensions of the scattering volume are approximately $1.5\times1.5\times3.5$ mm; the two equal dimensions are determined by the collimator C_3 of the primary beam while the greater one, along the primary beam direction, is given by the dimension of the secondary source.

The scattered atoms are detected with the bolometer B (width 0.3 mm, height 3 mm) cooled at 1.6 °K. The detector can be rotated around the direction of the secondary beam and is located 60 mm from the center of the scattering volume. Signal integration is performed with standard lock-in techniques.

Full experimental details will be published in the future. We briefly outline the three main techniques employed in this experiment.

A. Magnetic velocity selector

A velocity filter is realized using the focusing effect of an hexapolar magnetic field on paramagnetic atoms. At high field strengths ($B > 1.5$ kG for H atoms) the radial motion of the atomic hydrogen with electron spin antiparallel to the field direction is harmonic with frequency,[20]

$$\nu = \frac{1}{2\pi}(2\mu_B B_0/ma^2)^{1/2}, \tag{1}$$

where μ_B is the Bohr magneton, m is the atomic mass, a is the radial distance from the symmetry axis of the field of the expansion tip, and B_0 is the magnetic field at distance a.

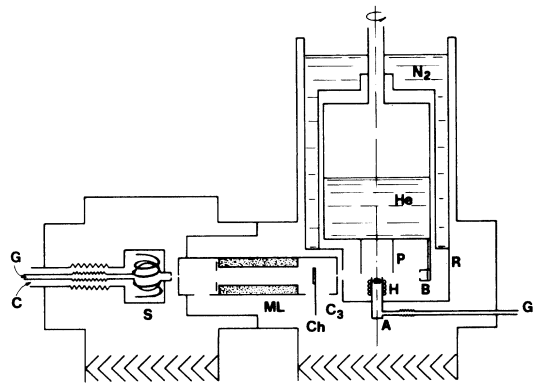

FIG. 1. Experimental apparatus. S is the rf discharge primary source, C the compressed-air cooling, G the gas inlet, ML the energy filter, C_3 the exit collimator of the energy filter, Ch the chopper, A the secondary source, H the heater, P the cryopump, He the liquid-helium bath, N_2 the liquid-nitrogen bath, R the radiation shield, and B the bolometer detector.

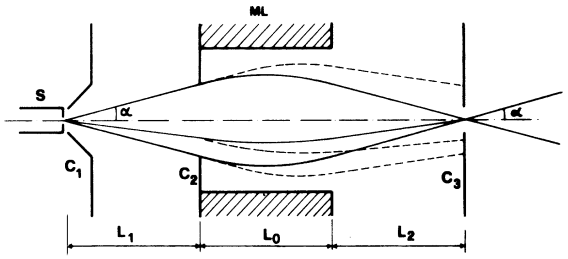

FIG. 2. Trajectories of particles of atomic hydrogen (or deuterium) in the hexapolar magnetic field. Solid lines correspond to the focused velocity, dashed lines to a nonfocused velocity. The lateral dimensions are greatly exaggerated. The geometry and characteristics of the velocity filter are reported in Table I.

Figure 2 shows in a meridian plane (a plane which contains the symmetry axis) the trajectories of particles emitted from a point source S located on the axis. For paraxial trajectories the wavelength in the field region

$$\Lambda = 2\pi a(E/\mu_B B_0)^{1/2} \tag{2}$$

depends on the energy and is independent of the mass of the particles. Atoms emitted by S with different velocities are focused at different points on the axis. The collimator C_3 selects particles with velocities in a given interval. Table I reports the relevant dimensions and characteristics of the energy filter.

The choice of equal free-flight distances L_1 and L_2 fixes the angular divergence of the velocity-selected beam to be equal to the divergence (controlled by the collimator C_2) of the beam entering the magnet. For a given experimental condition the nominal focused velocity v_1 is determined by

TABLE I. Relevant dimensions and characteristics of the atomic beam energy filter.

C_1	diameter	0.28 mm
C_2	diameter	2.1 mm
C_3	diameter	0.28 mm
L_1	distance	75 mm
L_2	distance	75 mm
L_0	length of magnet	75 mm
a	gap radius of magnet	1.55 mm
B_0	magnetic field at a	7800 G
$\bar{v}_1$	most probable velocity (H)	3600 m/sec
$\bar{v}_1$	most probable velocity (D)	2560 m/sec
R	velocity resolution	10%
T	transmission (estimated)	50%
$\Delta\Omega_1$	beam divergence (H)	$5.3\ 10^{-4}$ sr
$\Delta\Omega_2$	beam divergence (H_2)	$1.2\ 10^{-6}$ sr

the ratio L_1/L_0, where L_0 is the length of the magnet; in our case we choose the experimental parameter such that the transmitted velocity almost coincides with the most probable velocity of the Maxwellian beam produced by the rf source S. The velocity resolution is given in a first approximation by d_1/d_2, where d_1 and d_2 are the diameters of the collimators C_1 and C_2.

Figure 3 shows the velocity distribution measured by a slotted-disk velocity selector of 8.5% resolution using a bolometer detector.[21] The actual velocity resolution of the beam is about 10% if the selector convolution is taken into account. The most probable velocity is determined with an error of 0.5% using a symmetric selector.[22]

The velocity-selected beam has an intensity greater than 10^{16} atoms sr^{-1} sec^{-1} and a divergence $\Delta\Omega_1$ of 5.3 10^{-4} sr. We estimate an intensity gain of about 50 with respect to a mechanically selected beam with equal velocity resolution and equal area in the scattering region.

The energy filter also purifies the beam from molecular hydrogen; the beam of undissociated hydrogen has its divergence $\Delta\Omega_2$ determined by the small aperture collimator C_3, and the sensitivity of the detector is about 20 times smaller for H_2 than for H beams.[23] The signal measured by the bolometer with the rf discharge off is about three orders of magnitude smaller than the signal with the rf on. Taking into account the dissociation degree of the source, we estimate that in the condition of the present experiment the Maxwellian beam of molecular hydrogen gives a signal about 10^4 times smaller than the velocity-selected H beam.

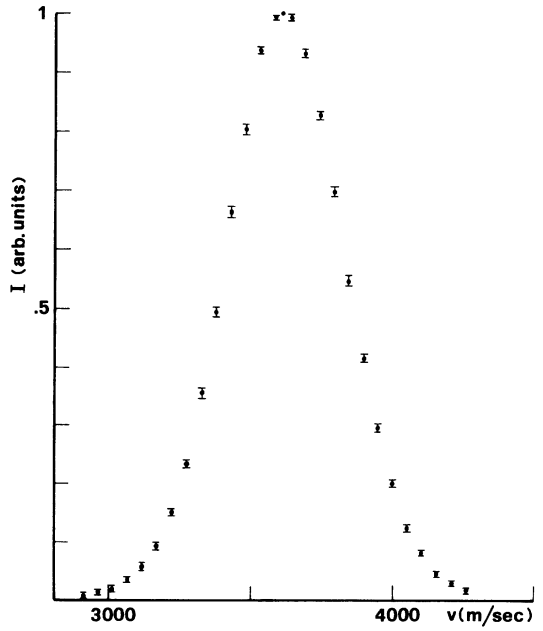

FIG. 3. Measured intensity I of the beam transmitted by the magnetic filter as a function of the velocity v.

B. Secondary beam

The secondary beam is produced by a glass multichannel source of 1.5×3.0 mm (the greater dimension is in the direction of the primary beam). The source is thermally connected to the liquid-nitrogen bath and its temperature, measured with a Au-Fe–Chromel thermocouple, can be controlled by the heater H.

The secondary beam can be displaced perpendicular to the primary beam in order to optimize the scattering rate. A typical attenuation is 30% with a negligible contribution from the background gas. No signal is detected at various angles when the secondary source is several millimeters away from the primary beam. The unusual high attenuations with negligible effect from the background are due to the high pumping efficiency of the directional cryopump P maintained at a temperature of 1.6 °K.

C. Detector

The detector is a commercially available 0.3×3 mm germanium bolometer (manufactured by Infrared Laboratory Inc.), which at the operating temperature of 1.6 °K has a noise-equivalent power of 10^{-13} $WHz^{-1/2}$.

This bolometer is a very sensitive detector for atomic hydrogen because the H atoms can either recombine on its surface or react with adsorbed molecules, releasing to the surface an energy which can be as large as 2.10^{-19} J/atom. Under the best conditions a beam of 5.10^6 atoms/sec gives a signal equal to the noise.

Previous experiments[23] on the responsivity of these bolometers to the H beams showed that a layer of oxygen molecules on its surface favors the recombination processes. The bolometer surface is therefore continuously covered at a rate of about 10^{-2} layer/sec by means of an auxiliary molecular oxygen beam. This also prevents surface changes which may arise either from adsorption of molecules of the target or from chemical reactions. In this way the maximum sensitivity coupled with a stable signal is achieved.

III. RESULTS

Experimental results for H-Ar and D-Ar are reported in Fig. 4. The experimental resolution allows us to resolve the fast oscillations of the differential cross section. The angular separation

between two successive extrema, of the order of some degrees, is proportional to the inverse of the reduced mass μ and of the relative velocity v, in agreement with the approximate equation[24]

$$\Delta\Theta = \pi\hbar/\mu v r_0, \tag{3}$$

where r_0 is the point where the potential is zero.

The relative collision energies for the two systems are almost equal (67.4 meV for H-Ar and 66.1 for D-Ar). They are calculated with the equation

$$E_r = \tfrac{1}{2}[m_1 m_2/(m_1+m_2)](\bar{v}_1^2+\bar{v}_2^2), \tag{4}$$

where m_1, $\bar{v}_1$ and m_2, $\bar{v}_2$ are the mass and the mean velocity of the primary and secondary beams, respectively. The quantity $K = \frac{1}{2}m_1\bar{v}_1^2$ is equal for the two systems because the hexapole behaves as an energy filter. The small difference in the relative energies for the two systems is due to the small difference between the reduced mass μ and the primary mass m_1 and to a small contribution of the secondary beam to the relative velocity.

The measured effective differential cross sections $I(\Theta)$, reported in Fig. 4, are the averages of some runs performed on different days. The error bar of each point $\mu(\theta)$ is the maximum difference between individual cross sections. Errors at small angles are due to the strong signal dependence on the angular position.

An individual cross section is the difference of the signal with secondary beam on (S) and off (S_0), respectively. The background signal S_0 is always less than 20% of the total signal S.

A run of 20 angular positions is measured in about $\frac{1}{2}$ h. All the experimental values are corrected for a drift smaller than 10% h^{-1} and averaged over two successive runs with increasing and decreasing angular positions, respectively. The primary beam attenuation is of the order of 30%. Attenuations ranging from 10% to 50% do not affect the behavior of the experimental curves.

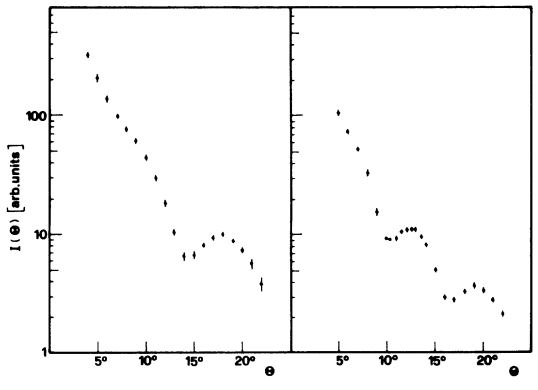

FIG. 4. Differential-cross-section measurements in arbitrary units as a function of the laboratory angle for H-Ar (left-hand side) and for D-Ar (right-hand side).

IV. ANALYSIS

For an assumed potential, differential cross sections are calculated by the partial-wave method using the JWKB approximation for phase shifts instead of the quantum-mechanical numerical integration of the radial Schrödinger equation. We checked that this approximation does not affect the analysis described below.

Calculated cross sections are converted into the laboratory system using Helbing's formulas[25] and averaged over the experimental conditions. The averaging is performed both over the velocity distribution and the angular divergence of the primary beam and over the scattering volume. Moreover, we have checked that the velocity distribution, the divergence of the secondary beam, and the detector dimensions give negligible contribution to the cross-section smearing.

We emphasize that in our experimental conditions the cross-section smearing essentially stems from well-known velocity distribution and angular

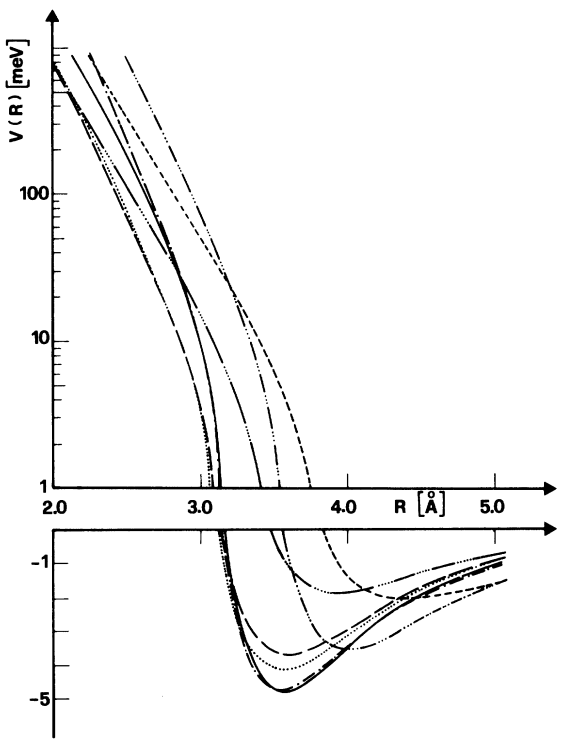

FIG. 5. H-Ar potential-energy curves. $P1$ (— ··· —) and $P2$ (----) are derived from the experiment of Aquilanti *et al.* (Ref. 14); $G1$ (— · —) and $G2$ (———) from the experiment of Bickes *et al.* (Ref. 15); MCSCF (·····), SCFC8 (— — —), and SCFC6 (— ····· —) are the three theoretical potentials of Wagner *et al.* (Ref. 4).

TABLE II. Most relevant potential parameters and K_t value [see Eq. (7)] normalized to the BF potential (K_t').

Potential	ϵ (meV)	r_m (Å)	r_0 (Å)	K_t'	Ref.
$G1$ LJ (12-6)	4.73	3.54	3.15	2.35	15
$G2$ exp $(\alpha,6)$	4.80	3.56	3.17	1.90	15
$P1$ LJ (12-6)	3.56	4.00	3.56	34.8	14
$P2$ LJ (8-6)	2.06	4.40	3.80	52.8	14
MCSCF	4.16	3.57	3.10	1.86	4
SCFC8	3.72	3.60	3.13	1.81	4
SCFC6	1.85	3.94	3.47	17.5	4
BF modified MCSCF	4.16	3.62	3.15	1.00	This work

divergence of the primary beam, while the smearing is generally determined by the secondary beam whose characteristics are difficult to measure.

V. COMPARISON WITH PREVIOUS WORK

A. Experimental studies

The best-fit potentials derived from total-collision-cross-section measurements at thermal energies[14,15] are reported in Fig. 5. Values of potential parameters are reported in Table II.

Two different analytical forms are used in the above references, a two-parameter Lennard-Jones (LJ) model,

$$V(r)=[6\epsilon/(n-6)][(r_m/r)^n-\tfrac{1}{6}n(r_m/r)^6], \quad (5)$$

and a three-parameter Slater-Buckingham exp$(\alpha,6)$ model,

$$V(r)=\frac{\epsilon}{1-6/\alpha}\left[\frac{6}{\alpha}\exp\left(\alpha-\frac{\alpha r}{r_m}\right)-\left(\frac{r_m}{r}\right)^6\right]. \quad (6)$$

Potentials derived in Ref. 15 generate cross sections in fairly good agreement with our data (see Fig. 6). In particular the location of the extrema are predicted with great accuracy, but the experimental points are lower than the computed curves at small angles and the relative heights of extrema are inaccurately reproduced.

The two best-fit potentials of Ref. 15—a LJ (12-6) and an exp$(\alpha,6)$, hereafter referred to as $G1$ and $G2$, respectively—are almost equal and therefore give similar cross sections. For clarity only the exponential curve is reported in Fig. 6.

The two potentials LJ (12-6) and LJ (8-6), proposed in Ref. 14, yield cross sections in disagreement with our data. The calculated extrema are shifted at very small angles and a smaller r_0 value is needed to reproduce the extrema positions. A reduction of r_0 implies a reduction of the absolute total cross section (roughly $\Delta\sigma/\sigma=2\Delta r_0/r_0$) in better agreement with the absolute value measured by Bickes *et al.*[26]

B. Theoretical studies

The H-Ar interaction at intermediate and long-range separation was recently calculated by Wagner, Das, and Wahl[4] with multiconfiguration self-consistent field (MCSCF) techniques previously used for systems with a considerably weaker interaction.

The interaction is computed at five internuclear

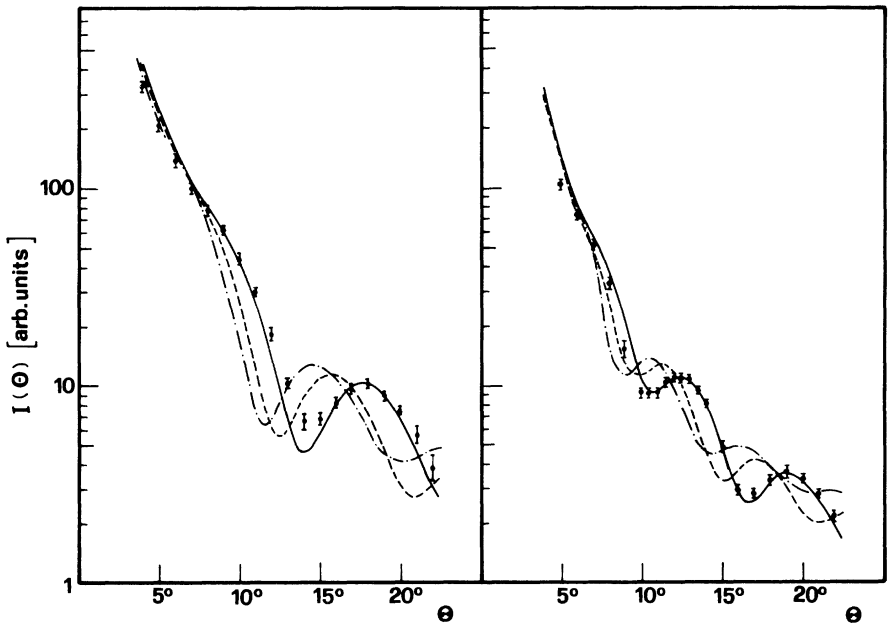

FIG. 6. Experimental points (•) compared with the effective differential cross sections calculated with the potentials derived from total-cross-section experiments. (———) pot. $G2$, (- - - -) pot. $P1$, (—·—·—) pot. $P2$. Potential parameters are reported in Table II.

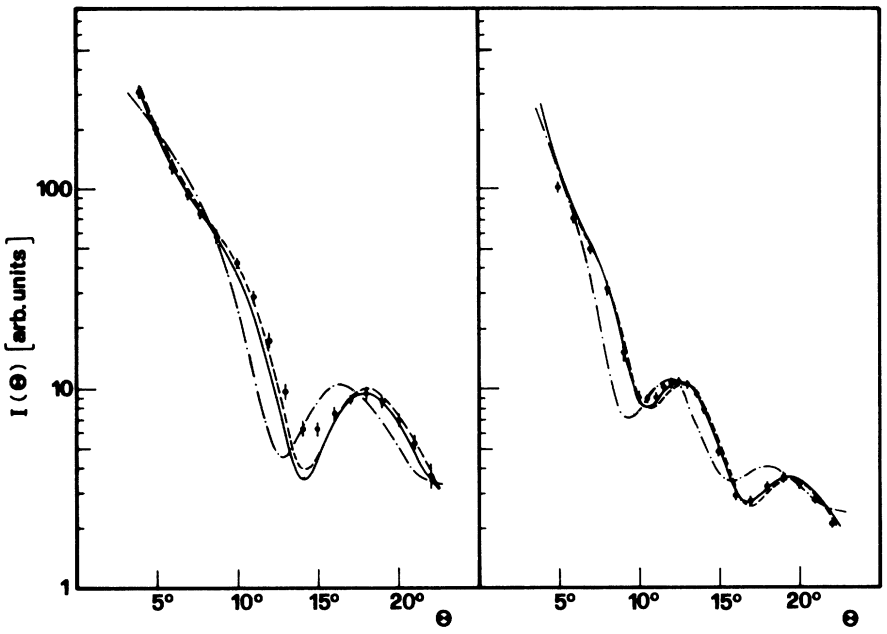

FIG. 7. Experimental points (•) compared with effective differential cross sections calculated with the theoretical potentials. (———) MCSCF, (— · —) SCFC6, (- - - -) SCFC8.

distances. The C_6 and C_8 values derived by the dispersion terms of this potential are in good agreement with long-range theoretical calculations.[27]

These authors suggest an analytical form (MCSCF potential) which fits the calculated values and assume an exponential repulsion. They propose also two approximate analytical potential curves (SCFC6 and SCFC8 using their notations) which fit the sum of the self-consistent-field part of the interaction and the dispersion energy obtained with negligible overlap effect. The SCFC6 potential contains only the C_6 term; the SCFC8 potential contains both the C_6 and C_8 terms.

The three potentials are reported in Fig. 5 and their most relevant parameters are given in Table II. The SCFC8 is similar to the MCSCF, but with a well depth 10% smaller. The SCFC6 is quite different, indicating that the C_8-term contribution is important at intermediate distances.

Effective differential cross sections generated by these potentials are reported in Fig. 7. The MCSCF curves reproduce our data quite well but

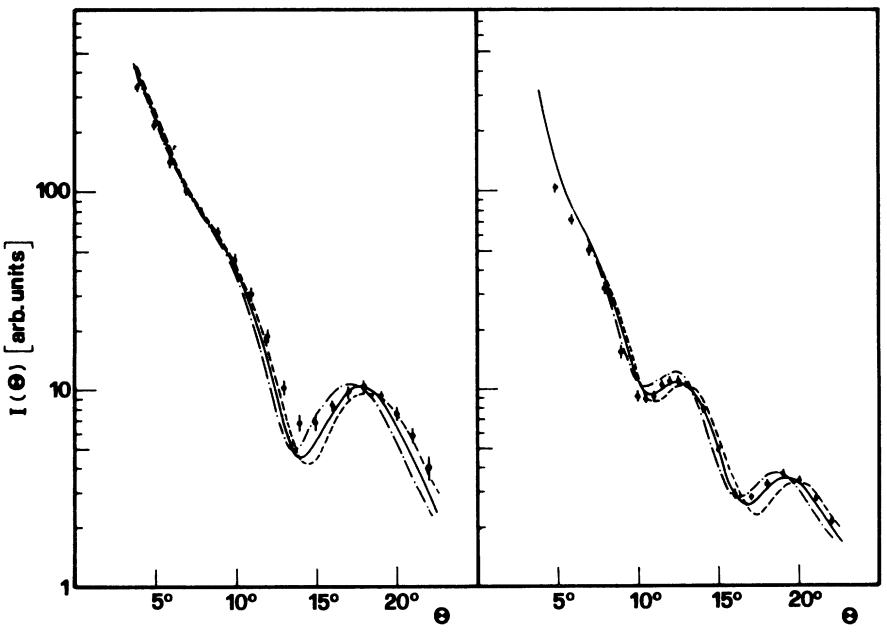

FIG. 8. Effective differential cross sections calculated with LJ (12-6) potentials with equal-strength parameter ϵr_m (16.9 meV Å). (———) r_m=3.54 Å, (- - - -) r_m=3.42 Å, (— · —) r_m=3.66 Å.

do not predict accurately the extrema positions for D-Ar in particular. The SCFC8 curves are similar, but the relative heights of the undulations are better fitted by the MCSCF potential.

VI. DISCUSSION

The angular positions of the fast undulations are mainly determined by the potential-range parameter r_0, in agreement with Eq. 3.

In Fig. 8 the present measurements are compared to the effective differential cross sections, assuming LJ (12-6) potentials with equal strength parameter. The solid curve is calculated by using potential parameters derived from the total-cross-section measurements of Bickes *et al.*[15] and the other two curves by using r_m values within the error limit given in their analysis. This figure is an example of the general fact that once an analytical form of the potential is assumed the present type of experiments greatly reduces the error limits of the parameter r_0 determined from total-cross-section measurements. Moreover, as far as the LJ (12-6) family of potentials is concerned, it is possible to reproduce angular positions of extrema (see solid curve) but not their relative amplitudes.

The influence of the negative and positive parts of the potential on the present data have been tested separately. Some trial potentials with equal repulsive and varying attractive parts (see Fig. 9) or equal attractive and varying repulsive parts (see Fig. 10) have been used. All the trial potentials have an exponential behavior for the repulsive part which is connected at the same r_0 to an attractive LJ (12-6) function or to a LJ (12-6) with one Gaussian modification.[28] Effective differential cross sections generated by these potentials are reported in Figs. 11 and 12, respectively. The analysis of these curves shows the following:

(a) The positions of the undulations in the investigated angular range are almost insensitive to the attractive and repulsive parts of the potential. Only the maximum located at about 20° of the D-Ar system is weakly sensitive to realistic modifications in the attractive part of the potential. Therefore the r_0 value, determined from the measured extrema, is essentially model independent.

(b) The cross sections at small angles are strongly influenced by the attraction and are insensitive to the repulsion. The form of the shoulder between 5° and 10°, measured with high

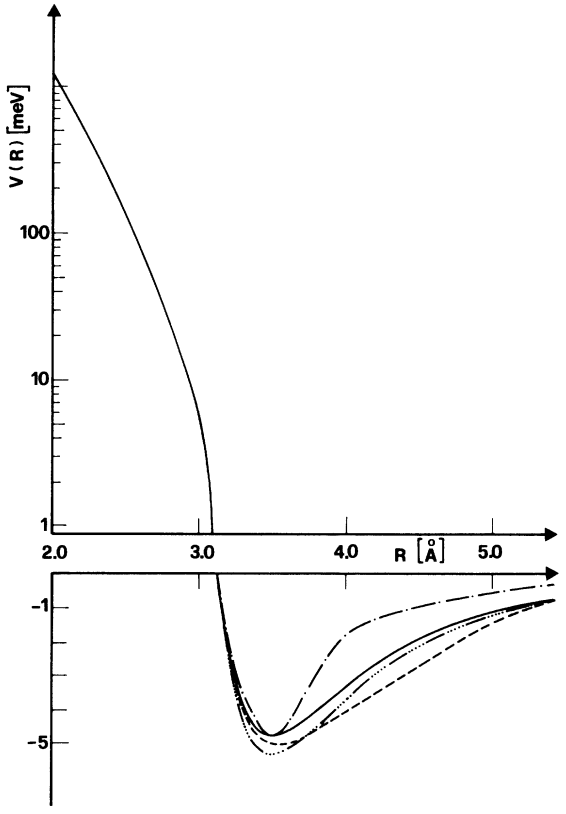

FIG. 9. Trial H-Ar potential-energy curves (see text).

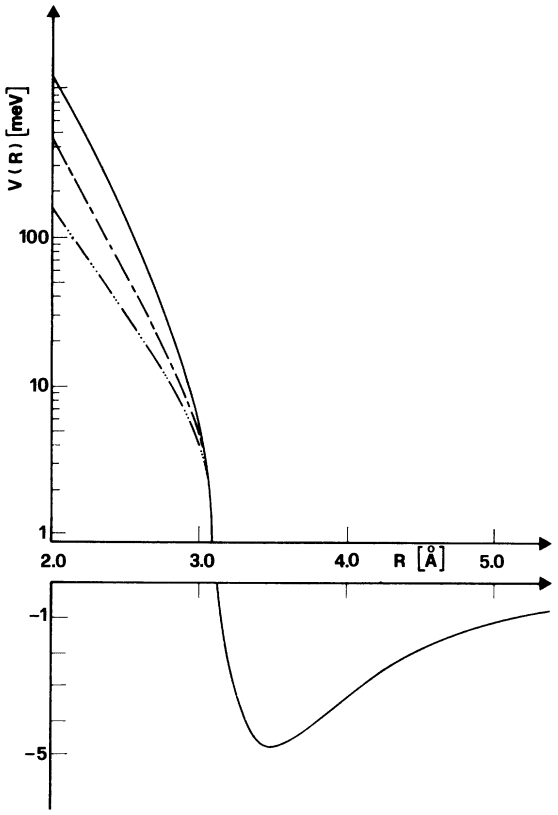

FIG. 10. Trial H-Ar potential-energy curves (see text).

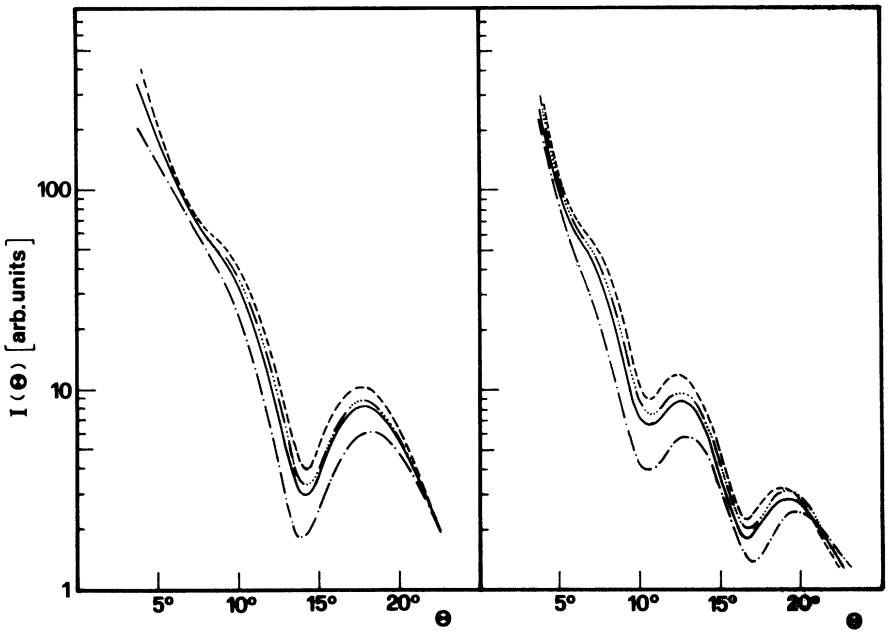

FIG. 11. Effective cross sections calculated with the potentials plotted with the same symbols in Fig. 9.

accuracy since the scattered intensities are high at these angles, may provide valuable information on the attractive interaction.

(c) The repulsive part of the potential has a greater influence on the D-Ar than on the H-Ar system.

(d) The relative heights of the undulations and background cross sections are influenced both by the attraction and by the repulsion. It is possible to obtain almost coincident relative differential cross sections with a suitable variation of both the attractive and repulsive parts of a given potential. Figure 13 reports almost coincident cross sections with the potentials plotted in Fig. 14, which are definitely different. Some differences at small angles are within the limits of experimental errors. The two cross sections are normalized because only relative measurements were performed; an absolute determination could discriminate between the curves.

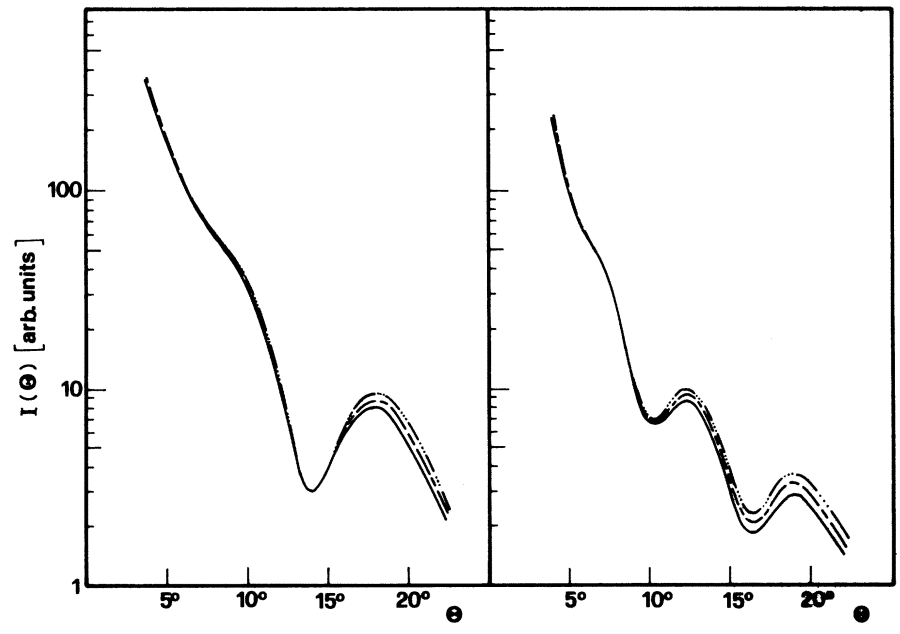

FIG. 12. Effective cross sections calculated with the potentials plotted with the same symbols in Fig. 10.

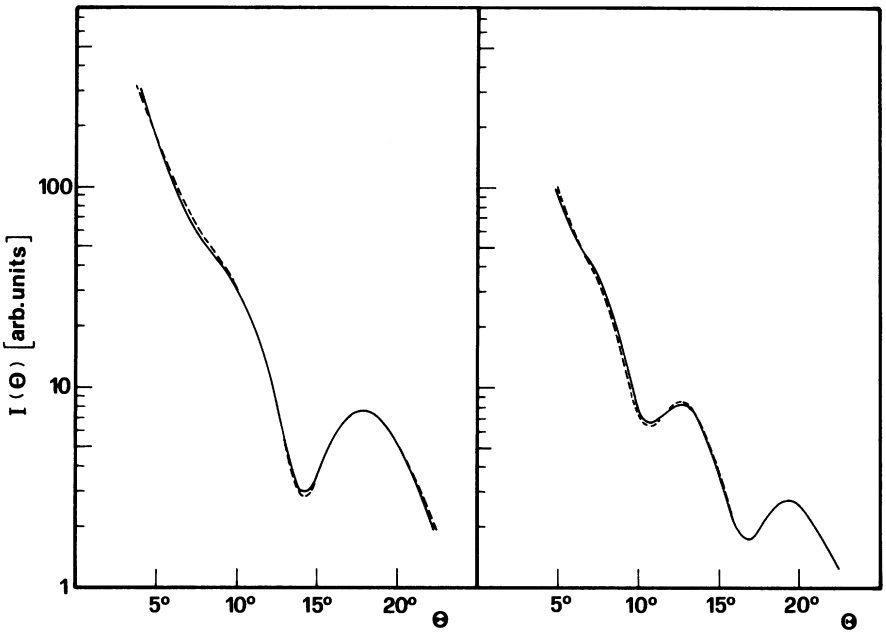

FIG. 13. Effective cross section calculated with the potentials plotted with the same symbols in Fig. 14.

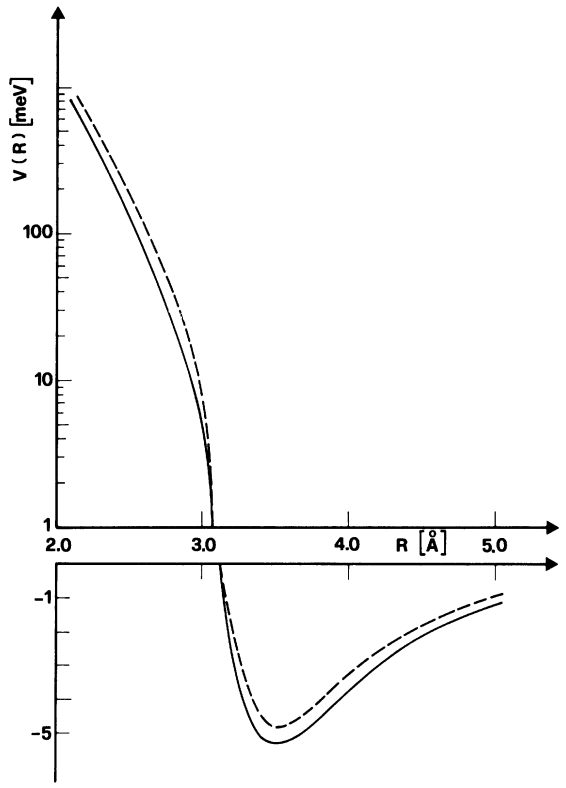

FIG. 14. Trial H-Ar potential-energy curves (see text).

A variety of about 30 numerical or analytical potentials has been used, the successive modifications on the potentials being guided by the discussion previously reported.

The quantity

$$K = \sum_{i=1}^{N} \left(\frac{Q_{\text{eff}}(\Theta_i) - AI(\Theta_i)}{A\mu(\Theta_i)} \right)^2 , \tag{7}$$

where A is the normalization parameter between the relative experimental intensity $I(\Theta)$ and the calculated effective cross section $Q_{\text{eff}}(\theta)$, and where $\mu(\theta)$ is the experimental error previously defined, is calculated for the systems H-Ar and D-Ar separately. The sum of the two K values (K_t) gives an indication of the validity of the fit. We note that the D-Ar data are more sensitive to the interaction potential than the H-Ar data because the experimental errors are smaller and more extrema are resolved for the heavier system.

We have not performed an automatic variation of the potential parameters in order to minimize K_t for two reasons: The experimental error is not the standard deviation of the measured intensities at each angle, so that statistical methods cannot be applied, and as suggested in the previous discussion, the measured properties cannot determine uniquely the potential form (see Figs. 13 and 14).

For a preliminary analysis a two-parameter LJ (12-6) potential was used but it does not prove sufficiently flexible to reproduce high-quality differ-

ential-cross-section measurements.[29]

Small modifications of the MCSCF potential proposed in Ref. 4 may improve the fit to our data. Figure 15 shows the best fit we have obtained; the calculated effective cross sections reproduce the D-Ar data very well and the H-Ar data fairly well. For the latter system the positions of the extrema and the background cross section are correct but the calculated relative amplitude of the extrema are too high. This discrepancy is present in all of the realistic potentials we have used.

The best-fit (BF) potential plotted in Fig. 16 is a modified MCSCF with an internuclear separation scale expanded 1.4% with respect to the original MCSCF and with an unchanged energy scale (see Table II). An equivalent fit can be obtained with proper simultaneous modifications both of the attractive and of the repulsive parts of the interaction (see Fig. 14). In Fig. 16 two potentials ($B1$ and $B2$) which give almost equivalent fit are also plotted; the K_t values for these two potentials are respectively 1.1 and 1.3 times greater than the K_t value for the BF potential.

VII. CONCLUSIONS

The two-parameter LJ-(12-6)-potential form, as deduced from the measurements of the energy dependence of the total collision cross section, is not flexible enough to reproduce our data. In fact, if the repulsive part of the BF potential is changed to agree with the best fit LJ(12-6) derived in Ref. 15, the attractive well must be even shallower (see Fig. 16).

The zero of the potential is the quantity most sensitive to the present data. The BF potential has an r_0 value equal to 3.15 Å; the $G1$ potential has the same r_0. This result suggests that the present measurements are highly consistent with the total-cross-section experiments of Ref. 15.

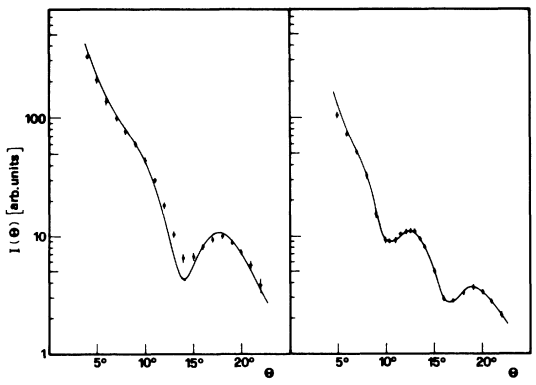

FIG. 15. Best-fit effective differential-cross-section curves. Best-fit potential is plotted in Fig. 16.

The error in the determination of r_0 is 0.03 Å, a factor 5 times smaller than the error derived from total-cross-section experiments.

The MCSCF potential has an r_0 value which is too small to reproduce the position of the extrema, but an expansion of 1.4% in the internuclear distance gives the BF potential. The analytical form proposed by Wagner *et al.*[4] in order to fit the theoretical values calculated in the well region therefore seems adequate to reproduce the interaction.

We have shown that different potential shapes can give almost equivalent cross sections. To better define a choice of the H-Ar potential, further experimental and theoretical work is needed. High-resolution differential-cross-section measurements at different energies and over an extended angular range will improve the knowledge of the H-Ar interaction.

Differential-cross-section measurements with a limited and known experimental smearing on systems with a small well capacity also seem suitable for testing quantum-inversion methods.[30]

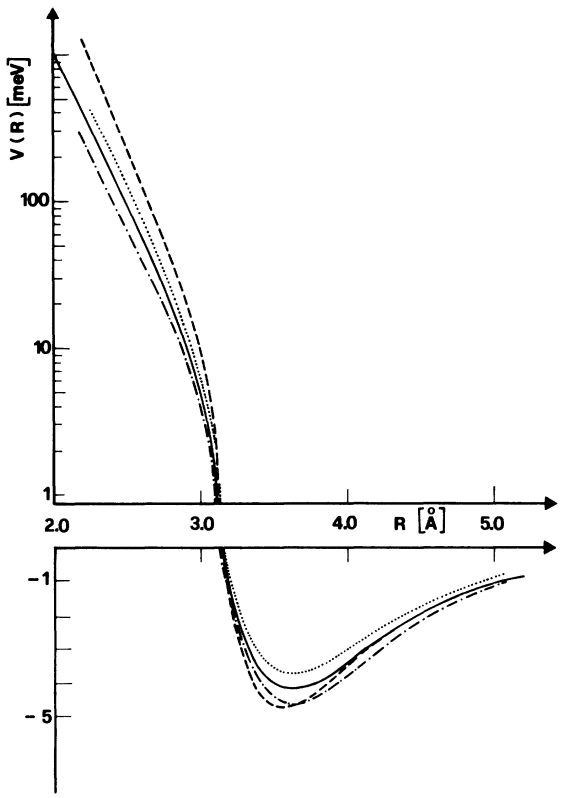

FIG. 16. Best-fit potential (———) compared with the LJ (12-6) potential ($G1$) derived from total-cross-section measurements of Ref. 15 (----) and with $B1$ (— · — ·) and $B2$ (· · · · ·) potentials which give an almost equivalent fit (see text).

*Work supported by the Italian National Research Council through the "Gruppo Nazionale di Struttura della Materia."

†Present address: Libera Università degli Studi di Trento, Facoltà di Scienze, Trento, Italy.

[1]P. J. Bertoncini and A. C. Wahl, Phys. Rev. Lett. 25, 991 (1970); J. Chem. Phys. 58, 1259 (1973); H. F. Schaefer, D. R. McLaughlin, F. E. Harris, and B. J. Alder, Phys. Rev. Lett. 25, 988 (1970); D. R. McLaughlin and H. F. Schaefer, Chem. Phys. Lett. 12, 245 (1971); B. Liu and D. McLean, J. Chem. Phys. 59, 4557 (1973).

[2]G. Das and S. Ray, Phys. Rev. Lett. 24, 1391 (1970).

[3]V. Bondybey, P. K. Pearson, and H. F. Schaefer, J. Chem. Phys. 57, 1123 (1972).

[4]A. F. Wagner, G. Das, and A. C. Wahl, J. Chem. Phys. 60, 1885 (1974).

[5]Ch. Schlier, Annu. Rev. Phys. Chem. 20, 191 (1969).

[6]W. E. Keller, *Helium 3 and Helium 4* (Plenum, New York, 1969).

[7]R. Feltgen, H. Pauly, F. Torello, and H. Vehmeyer, Phys. Rev. Lett. 30, 820 (1973).

[8]P. E. Siska, J. M. Parson, T. P. Schaefer, and Y. T. Lee, J. Chem. Phys. 55, 5762 (1971).

[9]R. Feltgen, K. A. Köhler, H. Pauly, F. Torello, and H. Vehmeyer, Proceedings of the IV International Symposium on Molecular Beams, Cannes, 1973, (unpublished), p. 304.

[10]The well-capacity parameter $B=2\mu\epsilon r_m^2\hbar^{-2}$ (μ is the reduced mass) is 5.5 and 7.4 for ^{3}He-^{3}He and ^{4}He-^{4}He, respectively. For comparison the B values are 27.6 and 54 for H-Ar and D-Ar, respectively.

[11]V. B. Leonas, Usp. Fiz. Nauk 107, 29 (1972) [Sov. Phys.—Usp. 15, 266 (1973)].

[12]Yu. N. Belyaev, N. V. Kamyshov, and V. B. Leonas, in *Proceedings of the Sixth International Conference on the Physics of Electronic and Atomic Collisions, Cambridge, Mass., 1969, Book of Abstracts* (MIT, Cambridge, 1969), p. 525.

[13]M. A. D. Fluendy, R. M. Martin, E. E. Muschlitz, and D. R. Herschbach, J. Chem. Phys. 46, 2172 (1967); W. C. Stwalley, A. Niehaus, and D. R. Herschbach, J. Chem. Phys. 51, 2287 (1969).

[14]V. Aquilanti, G. Liuti, F. Vecchio-Cattivi, and G. G. Volpi, Chem. Phys. Lett. 15, 305 (1972).

[15]R. W. Bickes, Jr., B. Lantzsch, J. P. Toennies, and K. Walaschewski, Discuss. Faraday Soc. 55, 167 (1973).

[16]R. Gengenbach, J. P. Toennies, W. Welz, and G. Wolf, in *Proceedings of the Eighth International Conference on the Physics of Electronic and Atomic Collisions, Belgrade, 1973, Book of Abstracts* (Institute of Physics, Belgrade, 1973), p. 31.

[17]J. P. Toennies, W. Welz, and G. Wolf, J. Chem. Phys. 61, 2461 (1974).

[18]A typical differential elastic cross section for atomic systems shows the fast oscillations superimposed on the supernumerary rainbows slow oscillations [see, for example, H. Pauly and J. P. Toennies, Adv. At. Mol. Phys. 1, 195 (1965)]. Systems with small well depth and small reduced mass do not present rainbows, but present widely spaced "fast" oscillations. A picture of the differential cross section as a function of the well-capacity parameter $B=2\mu\epsilon r_m^2/\hbar^2$ is reported by Farrar and Lee, J. Chem. Phys. 56, 5801 (1972).

[19]D. Bassi, M. G. Dondi, R. Penco, F. Tommasini, F. Torello, and U. Valbusa, in *Proceedings of the Fourth International Conference on Atomic Physics, Heidelberg, 1974, Abstracts of Contributed Papers* (Heidelberg U. P., 1974), p. 524.

[20]P. Kusch and V. W. Hughes, *Handbuch der Physik* (Springer-Verlag, Berlin, 1959), Vol. XXXVII/1, p. 1.

[21]A. Barcellona, M. G. Dondi, V. Lagomarsino, F. Tommasini, and U. Valbusa, Ref. 9, p. 443.

[22]See, for example, D. Beck, H. Dummel, and U. Henkel, Z. Phys. 185, 19 (1965).

[23]G. Marenco, A. Schutte, G. Scoles, and F. Tommasini, J. Vac. Sci. Technol. 9, 824 (1972).

[24]A. Kuppermann, R. J. Gordon, and M. J. Coggiola, Discuss. Faraday Soc. 55, 145 (1973).

[25]R. K. B. Helbing, J. Chem. Phys. 48, 472 (1968).

[26]Absolute values are the main source of information on the interaction derived by structureless total cross sections. A possible explanation for the disagreement between the potentials derived from two different total cross section measurements (Refs. 14 and 15) is in a systematic error in the absolute cross section, possibly greater than the quoted value [Aquilanti *et al.* (Ref. 14) give an error of 4%, Bickes *et al.* (Ref. 15) of about 2%].

[27]A. Dalgarno, Adv. Chem. Phys. 12, 143 (1967); W. B. Davidson, J. Phys. Chem. B 2, 1110 (1969); G. Starkschall, J. Chem. Phys. 56, 5728 (1972); W. C. Stwalley, *ibid.* 61, 3840 (1974); J. S. Cohen and R. T. Pack, *ibid.* 61, 2372 (1974).

[28]R. Düren, G. P. Raabe, and Ch. Schlier, Z. Phys. 214, 410 (1968).

[29]The r_0 parameter is determined with great accuracy from the location of the undulations while the well-depth parameter cannot account for the relative heights of the undulations and the general behavior of the cross sections for both systems (see also Fig. 8).

[30]For a review, see U. Buck, Rev. Mod. Phys. 46, 369 (1974).